



RESEARCH PAPER

Consideration of Fractional Distribution Parameter f_d in the Chen and Gross Method for Tissue-to-Plasma Partition Coefficients: Comparison of Several Methods

Yoo-Seong Jeong¹ · William J Jusko¹

Received: 2 December 2021 / Accepted: 17 February 2022 / Published online: 14 March 2022
© The Author(s), under exclusive licence to Springer Science+Business Media, LLC, part of Springer Nature 2022

Abstract

Purpose The tissue-to-plasma partition coefficient (K_p) describes the extent of tissue distribution in physiologically-based pharmacokinetic (PBPK) models. Constant-rate infusion studies are common for experimental determination of the steady-state $K_{p,ss}$, while the tissue-plasma concentration ratio (C_T/C_p) in the terminal phase after intravenous doses is often utilized. The Chen and Gross (C&G) method converts a terminal slope C_T/C_p to $K_{p,ss}$ based on assumptions of perfusion-limited distribution in tissue-plasma equilibration. However, considering blood flow (Q_T) and apparent tissue permeability ($f_{up}PS_{in}$) in the rate of tissue distribution, this report extends the C&G method by utilizing a fractional distribution parameter (f_d).

Methods Relevant PBPK equations for non-eliminating and eliminating organs along with lung and liver were derived for the conversion of C_T/C_p values to $K_{p,ss}$. The relationships were demonstrated in rats with measured C_T/C_p and $K_{p,ss}$ values and the model-dependent f_d for 8 compounds with a range of permeability coefficients. Several methods of assessing K_p were compared.

Results Utilizing f_d in an extended C&G method, our estimations of $K_{p,ss}$ from C_T/C_p were improved, particularly for lower permeability compounds. However, four in silico methods for estimating K_p performed poorly across tissues in comparison with measured K_p values. Mathematical relationships between K_p and $K_{p,ss}$ that are generally applicable for eliminating organs with tissue permeability limitations necessitates inclusion of an extraction ratio (ER) and f_d .

Conclusion Since many different types/sources of K_p are present in the literature and used in PBPK models, these perspectives and equations should provide better insights in measuring and interpreting K_p values in PBPK.

Keywords Physiologically-based pharmacokinetic (PBPK) modeling · tissue-to-plasma partition coefficient · tissue distribution rate · permeability coefficient

Introduction

Physiologically-based pharmacokinetics (PBPK) is a modeling approach that enables analysis and predictions of drug concentrations over time in plasma/blood and peripheral tissues. Among the key factors utilized in PBPK models, tissue-to-plasma partition coefficients (K_p) determine the extent of drug distribution to each tissue. The volume of distribution at steady-state (V_{SS}) is a function of K_p values for various organs (1–3). A typical PBPK equation for a

perfusion-limited and non-eliminating tissue based on the well-stirred organ model is (4, 5):

$$V_T \frac{dC_T}{dt} = Q_T \cdot R_b \cdot \left(C_p - \frac{C_T}{K_p} \right) \quad (1)$$

where C_T and C_p are the drug concentrations in tissue and arterial plasma (venous plasma for lung), V_T is the anatomical tissue volume, Q_T is the blood perfusion rate, and R_b is the blood-to-plasma partition coefficient. In Eq. 1, C_T/K_p denotes the outflow plasma concentration from the tissue (C_{out}) after drug partitioning, since the ratio C_T/C_{out} is expressed as:

✉ William J Jusko
wjusko@buffalo.edu

¹ Department of Pharmaceutical Sciences, School of Pharmacy and Pharmaceutical Sciences, State University of New York at Buffalo, 404 Pharmacy Building, Buffalo, NY 14214-8033, USA

$$K_p = \frac{C_T}{C_{out}} = \frac{\frac{C_{uT}}{f_{uT}}}{\frac{C_{up}}{f_{up}}} = \frac{PS_{in} \cdot f_{up}}{PS_{out} \cdot f_{uT}} \quad (2)$$

where C_{uT} and C_{up} are unbound drug concentrations in tissue and plasma, f_{uT} and f_{up} are corresponding free fractions of drug, and PS_{in} and PS_{out} are permeability-surface area clearances of unbound compounds into and out of tissues. Based on the free drug hypothesis (6, 7), in vitro binding studies in plasma and tissue homogenates seeking f_{up} and f_{uT} with considerations of reliable dilution factors (8, 9) can be utilized for predictions of K_p and thus V_{SS} (10). Many in silico methods have been developed for predicting K_p values in different tissues using physicochemical properties of compounds such as log P and f_{up} (11–13) along with their ionization status (pKa) (14–16) to estimate tissue binding properties (f_{uT}), though such methods show only approximate agreement with direct experimental measurements. The main basis for these methods is that drug molecules are reversibly distributed into tissue-specific constituent(s) (e.g., lipids and/or proteins) by passive diffusion (i.e., symmetrical movement of unbound drugs across the tissue membrane; $PS_{in} = PS_{out}$), such that the term K_p in Eq. 2 is expressed as the ratio f_{up}/f_{uT} . When active transport mechanisms (17, 18) are significant, the concentration ratio of tissue (C_T) to plasma (C_{out}) would theoretically deviate from f_{up}/f_{uT} .

In practice, constant-rate drug infusion is necessary to reach steady-state for experimental determination of K_p values that are applicable for PBPK equations ($K_{p,ss}$; typically using arterial plasma), since the role of equilibration rate (e.g., $Q_T \cdot R_b$ for perfusion-limited distribution) is factored out at steady-state in Eq. 1. While the experimental $K_{p,ss}$ for non-eliminating organs represents K_p adopted in Eqs. 1 and 2, the $K_{p,ss}$ value determined for eliminating organs needs to be corrected by the extraction ratio (ER) to account for loss (19). For linear and stationary pharmacokinetics based on n -compartment models, n slopes (viz., n eigenvalues of the system matrix) are shared across all the plasma and tissues (20), which means that tissue concentration profiles in the terminal phase would decline in parallel with plasma profiles in semi-log plots. Therefore, tissue-to-plasma concentration ratios measured in this post-distributive phase after intravenous (IV) bolus injection (viz., C_T/C_p) are also useful for estimating K_p . This is especially so for a compound that has a long half-life that inconveniently requires a very long duration of infusion to reach steady-state or for a drug candidate with insufficient drug amount available in the early phase of drug development. To enhance the usefulness of measured C_T/C_p for estimating the ‘PBPK-applicable’ K_p , the Chen and Gross (C&G) method (21), has been used for theoretical conversion of a terminal slope C_T/C_p to $K_{p,ss}$ based on the assumption of perfusion-limited distribution. However, when considering both blood flow (Q_T) and apparent tissue

permeability ($f_{up}PS_{in}$) in the rate of tissue distribution (22, 23), the practical utility of the C&G method may be compromised for compounds with low permeability.

Therefore, the primary objective of this report is to propose extensions of the C&G method for determination of more reliable K_p estimates from IV bolus studies that are applicable for PBPK models, considering both Q_T and $f_{up}PS_{in}$ in the rate of tissue distribution. Previously, a fractional distributional parameter f_d was introduced to define the permeability limitations in tissue distribution processes in minimal PBPK (24) and whole-body PBPK models (22), where the product of Q_T and f_d denotes apparent distributional clearance (CL_{app}) to each tissue. An f_d can be reasonably calculated using f_{up} , R_b , and a permeability coefficient P obtained from a parallel artificial membrane permeability assay (PAMPA) (i.e., compound-specific) along with Q_T and the effective surface area across the interface between the systemic circulation and tissues (S_{eff}) of rats (i.e., system-specific). Utilizing f_d in an extended C&G method, we herein demonstrate the theoretical conversion of the terminal C_T/C_p to $K_{p,ss}$ measured for 8 compounds with a wide range of apparent PAMPA P coefficients. Since many different types of K_p are present in the literature and used in PBPK models, extended mathematical relationships were developed between K_p and $K_{p,ss}$ that are generally applicable for eliminating organs with a tissue permeability limitation, necessitating the use of ER and f_d . These experimental $K_{p,ss}$ values are also compared with values obtained using four in silico prediction methods (11–16).

Theoretical Considerations

Non-eliminating Organ

Kinetic assumptions applied for Eqs. 1 and 2 include (i) instant drug binding to biological constituents in plasma and tissues, (ii) rapid equilibrium between plasma and red blood cells, and (iii) well-stirred tissue compartments with no permeability limitation. Adding tissue permeability PS into Eq. 1 based on the previous literature (22, 24), a differential equation for non-eliminating organs utilizing f_d is:

$$V_T \frac{dC_T}{dt} = Q_T \cdot f_d \cdot R_b \cdot \left(C_p - \frac{C_T}{K_p} \right) \quad (3)$$

where all symbols are consistent with Eq. 1 and f_d incorporates PS as will be shown later. At steady-state, both sides of Eq. 3 become 0, providing:

$$K_p = K_{p,ss} = \frac{C_{T,ss}}{C_{p,ss}} \quad (4)$$

where $C_{T,ss}$ and $C_{p,ss}$ denote tissue and plasma concentrations at steady-state. Since no elimination term is included in Eq. 3, the $K_{p,ss}$ for non-eliminating organs represents K_p , the operative parameter in PBPK models. Based on linear pharmacokinetics that leads to a parallel decline in the terminal phase for tissue and plasma concentrations in semi-log plots (20), the terminal phase concentrations after an IV bolus administration are:

$$C_p = A \cdot e^{-\beta t} \tag{5a}$$

$$C_T = B \cdot e^{-\beta t} \tag{5b}$$

where A and B are the y-intercepts extrapolated from the terminal-phase concentration profiles in plasma and tissue, and β is the terminal phase slope. Utilizing Eqs. 5a and 5b, Eq. 3 can be expressed as:

$$V_T \cdot (-B \cdot \beta \cdot e^{-\beta t}) = Q_T \cdot f_d \cdot R_b \cdot \left(A \cdot e^{-\beta t} - \frac{B \cdot e^{-\beta t}}{K_p} \right) \tag{6}$$

Since $C_T/C_p = B/A$, the rearrangement of Eq. 6 results in:

$$K_p = K_{p,ss} = \frac{1}{\frac{C_p}{C_T} + \frac{V_T \beta}{Q_T f_d R_b}} \tag{7}$$

Equation 7 indicates that $K_{p,ss}$ (or K_p for a non-eliminating organ) can be converted from C_T/C_p , with the anatomical/physiological information (V_T and Q_T), in vivo (β determined from a series of blood samples after IV injection) and in vitro observations (f_d and R_b). Assuming that R_b and f_d are 1 in Eq. 7 leads to the same relationship derived by Chen and Gross (21).

Eliminating Organ

Similar to Eq. 3, a differential equation for an eliminating organ utilizing f_d is:

$$V_T \frac{dC_T}{dt} = Q_T \cdot f_d \cdot R_b \cdot \left(C_p - \frac{C_T}{K_p} \right) - CL_{u,int} \cdot f_{uT} \cdot C_T \tag{8}$$

where $CL_{u,int}$ is the intrinsic clearance for unbound drug in the eliminating organ (i.e., $C_{uT} = f_{uT} \cdot C_T$). At steady-state, both sides of Eq. 8 become 0, and the rearranged equation is:

$$K_p \neq K_{p,ss} = \frac{C_{T,ss}}{C_{p,ss}} = \frac{1}{\frac{1}{K_p} + \frac{CL_{u,int} f_{uT}}{Q_T f_d R_b}} \tag{9}$$

It should be noted that $K_{p,ss}$ is different from K_p due to the presence of the term $CL_{u,int} f_{uT} / (Q_T f_d R_b)$ in the denominator of Eq. 9 which rearranges to:

$$\frac{CL_{u,int} f_{uT}}{Q_T f_d R_b} = \frac{1}{K_{p,ss}} - \frac{1}{K_p} \tag{10}$$

Utilizing the same relationships of Eqs. 5a and 5b in Eq. 8 for eliminating organs, a differential equation for tissue distribution in the terminal phase slope is:

$$V_T \cdot (-B \cdot \beta \cdot e^{-\beta t}) = Q_T \cdot f_d \cdot R_b \cdot \left(A \cdot e^{-\beta t} - \frac{B \cdot e^{-\beta t}}{K_p} \right) - CL_{u,int} \cdot f_{uT} \cdot B \cdot e^{-\beta t} \tag{11}$$

and

$$\frac{C_T}{C_p} = \frac{B}{A} = \frac{1}{\frac{1}{K_p} + \frac{CL_{u,int} f_{uT} - V_T \beta}{Q_T f_d R_b}} \tag{12}$$

Melding Eq. 10 into Eq. 12 yields:

$$K_p \neq K_{p,ss} = \frac{1}{\frac{C_p}{C_T} + \frac{V_T \beta}{Q_T f_d R_b}} \tag{13}$$

In comparison of Eqs. 7 and 13, $K_{p,ss}$ could be converted from C_T/C_p by the same mathematical relationship, regardless of the presence of tissue elimination. As shown in Eq. 10, determinations of $CL_{u,int}$, f_{uT} , Q_T , f_d , and R_b along with the estimated $K_{p,ss}$ from Eq. 13 can lead to estimation of K_p from $K_{p,ss}$ for eliminating organs. Analogously, assuming R_b and f_d in Eq. 13 are equal to unity leads to the same relationship derived by Chen and Gross (21) for an eliminating organ.

Lung Tissue Case

The rates of drug distribution in the lung and arterial blood are expressed (e.g., lung as a non-eliminating organ) as:

$$V_{LU} \frac{dC_{LU}}{dt} = Q_{LU} \cdot f_{d,LU} \cdot R_b \cdot \left(C_{ven,p} - \frac{C_{LU}}{K_{p,LU}} \right) \tag{14a}$$

$$V_{art} \cdot R_b \cdot \frac{dC_p}{dt} = Q_{LU} \cdot R_b \cdot (C_{out,LU} - C_p) \tag{14b}$$

where LU , art , and p in the subscripts denote lung, arterial blood, and arterial plasma. The blood perfusion rate to lung is regarded as cardiac output ($Q_{LU} = Q_{CO}$). The $C_{ven,p}$ is the outflow plasma concentration from the venous blood pool that takes a role of input concentration into lung tissue. Stringently, therefore, PBPK-applicable $K_{p,LU}$ denotes the lung-to-‘venous’ plasma partition coefficient. Based on Fick’s law of perfusion in Eq. 14a, $C_{out,LU}$, the outflow plasma concentration from lung, is written as:

$$C_{out,LU} = C_{ven,p} \cdot (1 - f_{d,LU}) + \frac{C_{LU}}{K_{p,LU}} f_{d,LU} \quad (15)$$

At steady-state, both sides of Eqs. 14a and 14b become 0 (i.e., $C_{p,ss} = C_{out,LU,ss} = C_{ven,p,ss}$), and rearrangement leads to:

$$K_{p,LU} = K_{p,LU,ss} = \frac{C_{LU,ss}}{C_{p,ss}} = \frac{C_{LU,ss}}{C_{ven,p,ss}} \quad (16)$$

In the terminal phase after an IV bolus injection with the slope β , the division of both sides of Eq. 14a by C_{LU} results in:

$$\frac{V_{LU} \cdot (-\beta)}{Q_{LU} f_{d,LU} R_b} = \frac{C_{ven,p}}{C_{LU}} - \frac{1}{K_{p,LU}} \quad (17)$$

Based on Fick's law of perfusion, Eq. 14a after a bolus injection can be also re-written using Eq. 15 as:

$$\frac{V_{LU} \cdot (-\beta)}{Q_{LU} \cdot R_b} = \frac{C_{ven,p} - C_{out,LU}}{C_{LU}} \quad (18)$$

In addition, Eq. 14b can be expressed by rearrangements as:

$$\frac{V_{art} \cdot (-\beta)}{Q_{LU}} = \frac{C_{out,LU} - C_p}{C_p} \quad (19a)$$

$$C_{out,LU} = C_p \cdot \left(1 + \frac{V_{art} \cdot (-\beta)}{Q_{LU}} \right) \quad (19b)$$

From the mathematical relationships in Eqs. 17 to 19, $K_{p,LU}$ is:

$$K_{p,LU} = \frac{1}{\frac{C_p}{C_{LU}} \cdot \left(1 - \frac{V_{art}\beta}{Q_{LU}} \right) + \frac{V_{LU}\beta}{Q_{LU}R_b} \cdot \left(\frac{1}{f_{d,LU}} - 1 \right)} \quad (20)$$

The application of the perfusion-limited model in Eq. 20 ($f_{d,LU} = 1$) leads to a mathematical relationship consistent with the C&G method (21).

$$V_{LI} \cdot (-\beta) = \left\{ (Q_{LI} - Q_{SP} - Q_{GU}) + Q_{SP} \cdot \left((1 - f_{d,SP}) + \frac{C_{SP}}{C_p} \frac{1}{K_{p,SP}} f_{d,SP} \right) + Q_{GU} \cdot \left((1 - f_{d,GU}) + \frac{C_{GU}}{C_p} \frac{1}{K_{p,GU}} f_{d,GU} \right) \right\} \cdot \frac{C_p}{C_{LI}} R_b \cdot f_{d,LI} - Q_{LI} f_{d,LI} R_b \frac{1}{K_{p,LI,ss}} \quad (25)$$

Liver Compartment Connected to Spleen and Gut

In the physiology of the body, the outflow blood from the splanchnic tissues including gut and spleen enters the liver via the hepatic portal vein while the remaining (circa 40% for rat and 20% for man) liver blood flow (25) comes from the hepatic artery. The equations for the rate of drug distribution to the liver, gut, and spleen are defined in whole-body PBPK as (22):

$$V_{LI} \frac{dC_{LI}}{dt} = Q_{LI} \cdot f_{d,LI} \cdot R_b \cdot \left(C_{in,LI} - \frac{C_{LI}}{K_{p,LI}} \right) - CL_{u,li} \cdot f_{u,LI} \cdot C_{LI} \quad (21a)$$

$$V_{GU} \frac{dC_{GU}}{dt} = Q_{GU} \cdot f_{d,GU} \cdot R_b \cdot \left(C_p - \frac{C_{GU}}{K_{p,GU}} \right) \quad (21b)$$

$$V_{SP} \frac{dC_{SP}}{dt} = Q_{SP} \cdot f_{d,SP} \cdot R_b \cdot \left(C_p - \frac{C_{SP}}{K_{p,SP}} \right) \quad (21c)$$

where LI , GU , and SP in the subscripts denote liver, gut, and spleen. The $C_{in,LI}$ is the plasma concentration entering the liver, expressed as:

$$C_{in,LI} = \frac{(Q_{LI} - Q_{SP} - Q_{GU}) \cdot C_p + Q_{SP} \cdot C_{out,SP} + Q_{GU} \cdot C_{out,GU}}{Q_{LI}} \quad (22)$$

where $C_{out,SP}$ and $C_{out,GU}$ are the outflow plasma concentrations from spleen and gut. Since $C_{in,SP} = C_{in,GU} = C_p$ as shown in Eqs. 21b and 21c, $C_{out,SP}$ and $C_{out,GU}$ can be written, based on Fick's law of perfusion in Eqs. 21b and 21c, as:

$$C_{out,SP} = C_p \cdot (1 - f_{d,SP}) + \frac{C_{SP}}{K_{p,SP}} f_{d,SP} \quad (23a)$$

$$C_{out,GU} = C_p \cdot (1 - f_{d,GU}) + \frac{C_{GU}}{K_{p,GU}} f_{d,GU} \quad (23b)$$

At steady-state, both sides of Eqs. 21a to 21c are 0, which leads to the relationship of $C_{out,SP,ss} = C_{out,GU,ss} = C_{p,ss}$ from Eqs. 23a and 23b, and thereby $C_{in,LI,ss} = C_{p,ss}$ in Eq. 22. Therefore, the differential equation for the liver compartment at steady-state can be rearranged as:

$$K_{p,LI} \neq K_{p,LI,ss} = \frac{C_{LI,ss}}{C_{p,ss}} = \frac{1}{\frac{1}{K_{p,LI}} + \frac{CL_{u,li} f_{u,LI}}{Q_{LI} f_{d,LI} R_b}} \quad (24)$$

Utilizing drug concentrations in arterial plasma (C_p), liver (C_{LI}), spleen (C_{SP}), and gut (C_{GU}) in the terminal phase (with the same slope of β) after an IV bolus injection, the rearrangement of Eq. 21a with Eq. 24 yields:

From Eqs. 21b and 21c, the equations for the spleen and gut in the terminal phase after IV bolus injection are:

$$V_{SP} \cdot (-\beta) = Q_{SP} \cdot f_{d,SP} \cdot R_b \cdot \left(\frac{C_p}{C_{SP}} - \frac{1}{K_{p,SP}} \right) \quad (26a)$$

$$V_{GU} \cdot (-\beta) = Q_{GU} \cdot f_{d,GU} \cdot R_b \cdot \left(\frac{C_p}{C_{GU}} - \frac{1}{K_{p,GU}} \right) \quad (26b)$$

Application of Eqs. 26a and 26b in Eq. 25 leads to:

$$K_{p,LI,ss} = \frac{1}{\frac{C_p}{C_{LI}} \cdot \left(1 + \frac{V_{SP}\beta(C_{SP}/C_p) + V_{GU}\beta(C_{GU}/C_p)}{Q_{LI}R_b} \right) + \frac{V_{LI}\beta}{Q_{LI}f_{d,LI}R_b}} \quad (27)$$

Plugging the value of 1 into R_b and f_d in Eq. 27 for the case of $K_{p,LI} = f_{up}/f_{u,LI}$ (viz., symmetrical transport) in Eq. 24 leads to the C&G equation (21).

Theoretical Conversion of $K_{p,ss}$ to K_p Using f_d and Extraction Ratio (ER)

An estimated $K_{p,ss}$ as discussed above needs to be corrected to the ‘true’ or operative K_p that is applicable in PBPK equations for eliminating organs. Based on Fick’s law of perfusion, Eq. 8 can be re-written by utilizing C_{in} and C_{out} terms (with regard to plasma concentration) as:

$$V_T \frac{dC_T}{dt} = Q_T \cdot R_b \cdot (C_{in} - C_{out}) - CL_{u,int} \cdot f_{uT} \cdot C_T \quad (28)$$

In the typical well-stirred model (26), elimination rate is kinetically driven by C_{out} where the elimination term in Eq. 28 is replaced with $CL_{u,int} \cdot f_{up} \cdot C_{out}$ under the assumption that $f_{up} \cdot C_{out} = C_{uT}$. However, the unbound concentrations between plasma and tissue are not the same when $PS_{in} \neq PS_{out}$. Eqs. 8 and 28 are thus based on considering C_{uT} as the driving concentration for elimination in tissues. When Eq. 10 is rearranged:

$$K_p = \frac{1}{\frac{C_{p,ss}}{C_{T,ss}} - \frac{CL_{u,int}f_{uT}}{Q_T f_d R_b}} = \frac{Q_T f_d R_b \cdot C_{T,ss}}{Q_T f_d R_b \cdot C_{p,ss} - CL_{u,int} f_{uT} \cdot C_{T,ss}} \quad (29)$$

At steady-state, both sides of Eq. 28 are zero, resulting in:

$$K_p = \frac{Q_T f_d R_b \cdot C_{T,ss}}{Q_T f_d R_b \cdot C_{p,ss} - Q_T \cdot R_b \cdot (C_{in,ss} - C_{out,ss})} = \frac{C_{T,ss}}{C_{p,ss}} \cdot \frac{f_d}{f_d - \frac{C_{in,ss} - C_{out,ss}}{C_{p,ss}}} = K_{p,ss} \cdot \frac{1}{1 - ER/f_d} \quad (30)$$

where $C_{in,ss} = C_{p,ss}$ and ER is the traditionally defined extraction ratio (4). Based on Eq. 30, for example in liver, the relationship $K_{p,ss} = K_p \cdot (1 - ER) = K_p \cdot Q_{LI}/(Q_{LI} + f_{up} CL_{u,int}/R_b)$ (19) is only applicable for the well-stirred perfusion-limited liver model (26) with $f_{d,LI} = 1$.

Methods

Application of the Extended Chen and Gross Method for Eight Compounds in Rats

Rats are widely used for experimental determination of tissue partitioning properties, e.g., $K_{p,ss}$ from infusion studies and C_T/C_p from an IV bolus injection. Measured data for

both $K_{p,ss}$ and C_T/C_p in available tissues of rats were collected for 8 compounds (cefazolin, cyclosporine, dexamethasone, etoposide, furosemide, methotrexate, propranolol, and quinidine) as summarized in Tables I (for $K_{p,ss}$) and II (for C_T/C_p). If numerical tissue distribution data were not directly available from the literature, plasma/blood and tissue concentration profiles were digitized from published graphs using GetData Graph Digitizer version 2.26 (<http://getdata-graph-digitizer.com/>). The C_T/C_p data for dexamethasone at 24 h after a subcutaneous bolus administration were available from our recent study (27). For etoposide, methotrexate, and propranolol, terminal phase slopes were assumed to be the same between plasma and all tissues. Concentration-time profiles of dexamethasone in plasma and various tissues (27) experimentally showed parallel declines when plotted in semi-log graphs, providing adequate justification of using the same slope for different tissues. When terminal phase tissue slopes appear to be different from plasma/blood (for furosemide, cefazolin, cyclosporine, and quinidine), the assumption of linear pharmacokinetics leads to adoption of the terminal phase slope of tissue profiles (β_T), where Eqs. 7 and 13 for typical tissues, Eq. 20 for lung, and Eq. 27 for liver can be expressed as:

$$K_{p,ss} = \frac{1}{\frac{C_p}{C_T} + \frac{V_T \beta_T}{Q_T f_d R_b}} \quad (31a)$$

$$K_{p,LU} = \frac{1}{\frac{C_p}{C_{LU}} \cdot \left(1 - \frac{V_{art}\beta}{Q_{LU}} \right) + \frac{V_{LU}\beta_{LU}}{Q_{LU}R_b} \cdot \left(\frac{1}{f_{d,LU}} - 1 \right)} \quad (31b)$$

$$K_{p,LI,ss} = \frac{1}{\frac{C_p}{C_{LI}} \cdot \left(1 + \frac{V_{SP}\beta_{SP}(C_{SP}/C_p) + V_{GU}\beta_{GU}(C_{GU}/C_p)}{Q_{LI}R_b} \right) + \frac{V_{LI}\beta_{LI}}{Q_{LI}f_{d,LI}R_b}} \quad (31c)$$

where β , β_{LU} , β_{SP} , β_{GU} , and β_{LI} reflect the terminal phase slopes in arterial plasma, lung, spleen, gut, and liver. Eqs. 31a to 31c are derived in the same manner as done for Eqs. 7, 13, 20, and 27, except that the tissue concentration at the observed point (Eq. 5b) is replaced with the relationship $C_T = B \cdot e^{-\beta_T t}$. It was assumed that elimination kinetics did not take place in lung tissue for the 8 compounds assessed ($K_{p,LU} = K_{p,LU,ss}$).

Tissue partitioning properties were reported as tissue-to-blood concentration ratio for dexamethasone (C_T/C_B) and cyclosporine (C_T/C_B and $C_{T,ss}/C_{B,ss}$) (27, 32, 34). Based on the assumption of rapid equilibrium between plasma and red blood cells, the C_T/C_B at 24 h after a subcutaneous bolus injection of dexamethasone was converted to C_T/C_p by multiplication of R_b (0.725) and C_T/C_B values. Since two R_b

Table I Literature Data for $K_{p,ss}$ After Constant Infusion of 8 Compounds to Rats

$K_{p,ss}$	Furosemide	Cefazolin	Methotrexate	Etoposide	Dexamethasone	Cyclosporine (low dose) ^a	Cyclosporine (high dose) ^a	Propranolol	Quinidine
Source	Kitani et al. (1988) (28)	Tsuji et al. (1983) (29)	Yokooji et al. (2011) (30) ^b	Cárcel-Trullols et al. (2004) (31) ^b	Song et al. (2020) (27)	Bernareggi and Rowland (1991) (32)	Yata et al. (1990) (33)		
Adipose	–	–	–	–	0.16	13.9 ^c	29.6 ^c	–	–
Bone	–	0.111	–	–	0.19	2.45	3.44	–	–
Brain	0.0115	–	0.00490	–	0.06	–	0.159	14.0	0.9
Gut	0.517	0.114	0.142 ^d	5.98	0.82	5.51	7.70	6.6	10.1
Heart	–	0.101	0.122	0.722	0.84	3.27	4.56	7.1	5.8
Kidney	1.36	0.867 ^e	1.61	0.905	1.24	7.35	8.52	15.3	20.7
Liver	0.330	0.740 ^e	0.915	1.43	5.06	12.4	11.6	2.63 ^e	2.84 ^e
Lung	–	0.154	0.145	0.89	0.50	5.71	7.11	54.2	43.0
Muscle	0.164	0.077	0.0349	0.715	0.49	1.31	2.44	4.3	4.3
Skin	–	0.303	–	–	0.30	3.88	3.00	–	–
Spleen	–	–	0.0876	0.658	0.63	11.6	14.2	14.2	24.0

^aThe values for cyclosporine denote tissue-to-blood partition coefficient at steady-state, with the lower and higher dosages of 2.72 and 13.9 mg/kg/day

^bThe data were digitized from published graphs

^cThe adipose-to-blood concentration ratio at steady-state is the averaged values between dorsal and perirenal fat tissues

^dThe value for colon tissue

^eDetailed calculations are described in the text

values were available for cyclosporine depending on the infusion rate (e.g., 1.28 for lower dose and 1.18 for higher dose) (32), the reported C_T/C_B and $C_{T,ss}/C_{B,ss}$ are used without further correction with R_b as noted in Tables I and II. In this case, tissue-to-blood partition coefficients at steady-state ($K_{p,TB,ss}$) for typical tissues, lung, and liver are expressed as:

$$K_{p,TB,ss} = \frac{1}{\frac{C_B}{C_T} + \frac{V_T \beta_T}{Q_T f_d}} \quad (32a)$$

$$K_{p,TB,LU} = \frac{1}{\frac{C_B}{C_{LU}} \cdot \left(1 - \frac{V_{art} \beta}{Q_{LU}}\right) + \frac{V_{LU} \beta_{LU}}{Q_{LU}} \cdot \left(\frac{1}{f_{d,LU}} - 1\right)} \quad (32b)$$

$$K_{p,TB,LI,ss} = \frac{1}{\frac{C_B}{C_{LI}} \cdot \left(1 + \frac{V_{SP} \beta_{SP} (C_{SP}/C_B) + V_{GU} \beta_{GU} (C_{GU}/C_B)}{Q_{LI}}\right) + \frac{V_{LI} \beta_{LI}}{Q_{LI} f_{d,LI}}} \quad (32c)$$

For cyclosporine, tissue-specific terminal phase slopes were available in the literature (34) (Table II). If all terminal phase slopes in blood and tissues could be assumed to be the same, then β_{LU} , β_{SP} , β_{GU} , and β_{LI} could be replaced with β in Eqs. 32a to 32c.

When necessary to calculate f_d for various tissues, two distribution models proposed in whole-body PBPK for rats (Fig. 1) were used (22) with f_d equations expressed as:

$$f_{d,Model1} = 1 - e^{-\frac{f_{up} \cdot P \cdot S_{eff}}{Q_T \cdot R_b}} \quad (33a)$$

$$f_{d,Model2} = \frac{f_{up} \cdot P \cdot S_{eff}}{Q_T \cdot R_b + f_{up} \cdot P \cdot S_{eff}} \quad (33b)$$

where distribution Model 1 is based on the capillary permeability model (e.g., TUBE model) (38, 39) and the vascular compartment of Model 2 (e.g., JAR model) is a well-stirred compartment (23). The kinetics in the vascular compartment of the JAR model (viz., V_{vas}/Q_T) is assumed to be negligible to obtain Eq. 33b (22). From the derivation, it should be noted that the product $P \cdot S_{eff}$ in Eqs. 33a and 33b denotes the uptake clearance of unbound concentrations in plasma (PS_{in}) (22). Input parameters specific for the 8 compounds (9 cases with two dose levels for cyclosporine) are listed in Table III. System-specific input parameters (V_{art} , V_T , Q_T , and S_{eff}) for major tissues of rats with a typical body weight of 250 g are summarized in Table IV. Experimental $K_{p,ss}$ values were compared with C_T/C_p and those converted from the C&G method (i.e., perfusion-limited distribution) and Models 1 and 2. Since $K_{p,ss}$ is theoretically equivalent with AUC_T/AUC_p from a single dose study based on the assumption of linear pharmacokinetics, tissue concentration data as listed in Table II were also used for calculating AUC_T/AUC_p , where the initial concentration was set to be 0. Despite the limited tissue concentrations in the literature (40), the

Table II Literature Data Values of C_T/C_p After Bolus Injections of 8 Compounds to Rats. Terminal Phase Slopes for Plasma/Blood (β) and/or Tissues (β_T) are Included. The Same Sources Listed in Table I were Used Unless Otherwise Noted

C_T/C_p	Furosemide	Cefazolin ^a	Methotrexate ^b	Etoposide ^a	Dexamethasone ^c	Cyclosporine ^{a,b,d}	Propranolol ^b	Quinidine ^{a,b}
t_{last}	8 h	2 h	0.5 h	1 h	24 h	32 h	2 h	2.5 h
Adipose	–	–	–	–	0.357	41.5	–	4.59
Bone	–	0.125	–	–	1.12	5.55	–	–
Brain	0.0168 ^e	–	–	–	0.234	–	36.1	1.48
Gut	10.1	0.130	0.274 ^f	16.8	2.70	10.1	12.0	26.3
Heart	–	0.0940	0.282	0.792	1.89	8.55	8.66	16.1
Kidney	1.62	3.87	2.61	2.21	2.54	17.7	17.4	18.5
Liver	0.246	0.809	1.86	2.00	7.18	28.1	1.35 ^e	41.7
Lung	0.203	0.0927	0.274	1.29	1.53	17.7	99.9 ^h	70.8
Muscle	0.174	0.151	0.149	1.77	1.52	4.01	4.33	8.91
Skin	–	0.510	–	–	1.21	10.5	4.12	8.55
Spleen	–	–	0.122	0.892	1.63	17.6	24.7	48.5
β or β_T (h^{-1})								
Plasma	0.288	0.619	0.852 ⁱ	2.08 ⁱ	–	–	0.696 ⁱ	0.762
Blood	–	–	–	–	0.314 ⁱ	0.0753	–	–
Adipose	–	–	–	–	–	0.0304	–	0.558
Bone	–	0.497	–	–	–	0.0520	–	–
Brain	0.207	–	–	–	–	–	–	0.864
Gut	0.288 ⁱ	0.680	–	–	–	0.0512	–	0.126
Heart	–	0.718	–	–	–	0.0392	–	0.552
Kidney	0.257	0.616	–	–	–	0.0348	–	0.768
Liver	0.275	0.925	–	–	–	0.0380	–	0.108
Lung	0.288	0.817	–	–	–	0.0444	–	0.426
Muscle	0.201	0.317	–	–	–	0.0347	–	0.558
Skin	–	0.562	–	–	–	0.0263	–	0.414
Spleen	–	–	–	–	–	0.0529	–	0.270

^aThe data were digitized from the published graphs

^bThe data were obtained from different literature sources for methotrexate (35), cyclosporine (34), propranolol (36), and quinidine (37)

^c C_T/C_p was obtained from the multiplication of C_T/C_B and R_b for dexamethasone

^dThe values for cyclosporine denote tissue-to-blood concentration ratios

^e C_T/C_p determined at $t_{last} = 6$ h

^fThe value for large intestine

^g $\frac{C_{LI}}{C_p} = K_{p,LI,ss} \frac{Q_{LI}R_b + V_{SP}\beta(C_{SP}/C_p) + V_{GU}\beta(C_{GU}/C_p) + V_{ST}\beta(C_{ST}/C_p)}{Q_{LI}R_b - V_{LI}\beta K_{p,LI,ss}}$, where $K_{p,LI,ss} = K_{p,LI} \cdot (1 - ER)$ and $ER = 0.773$ (see text for details). Based on Shibasaki et al. (36), $K_{p,LI}$ was reported to be 5.45 and C_{ST}/C_p for stomach was calculated to be 6.37

^hFrom Eq. 20 with $f_{d,LU} = 1$, where $K_{p,LU}$ was reported to be 100.1 in Shibasaki et al. (36)

ⁱFor etoposide, dexamethasone, and cyclosporine, $\beta = \beta_T$ was assumed. β_{GU} for furosemide was not determined in the literature and assumed to be the same as β

data after an IV administration of propranolol at 1.5 mg/kg (with the terminal phase slope of 0.66 h^{-1}) were used for calculating AUC_T/AUC_p .

In addition, in silico K_p values were estimated by utilizing the physicochemical properties of the 8 compounds (Table III) with 4 different methods [i.e., Poulin and Theil (P&T) (11, 12), Berezhkovskiy (13), Rodgers and Rowland (R&R) (14, 15), and Lukacova (16), available from GastroPlus version 9.8.0002; Simulations Plus Inc., Lancaster,

CA]. The in silico K_p for gut tissue was calculated by Simcyp Simulator (Version 20 Release 1; Certara Ltd., Sheffield, UK), using Method 1 for P&T and Berezhkovskiy and Method 2 for R&R and Lukacova. For fair comparisons of $K_{p,ss}$ values in eliminating organs (e.g., liver and kidney), the in silico-predicted K_p values were corrected to $K_{p,ss}$ considering the experimental ER (calculated from organ clearances in Table IV) and the model-dependent f_d (from Eqs. 33a and 33b), based on the Eq. 30.

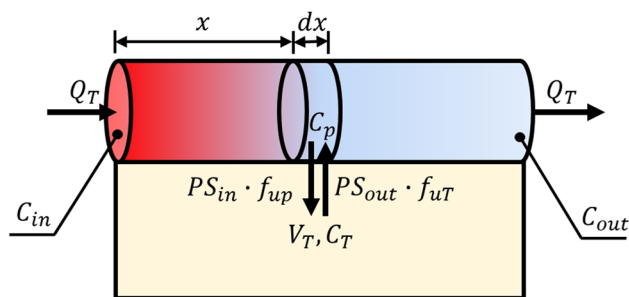
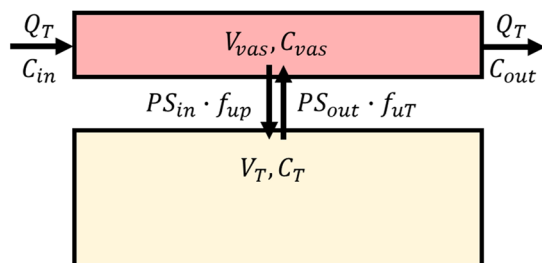
Model 1:**Model 2:**

Fig. 1 Structures of two distribution models used for calculation of f_d (22). Symbols for Models 1 and 2 are described in the text

Results**Refinement of Collected Data from the Literature**

Tsuji et al. (1983) (29) reported K_p values for cefazolin in liver (0.788) and kidney (2.79) of rats that differ from $K_{p,ss}$ where $K_{p,ss}$ was already corrected using an ER in those tissues. Since the steady-state arterial plasma concentration of cefazolin (i.e., free and bound) was 77.5 $\mu\text{g/mL}$, the f_{up} at steady-state was expected to be 0.163 with a C_{up} of 12.6 $\mu\text{g/mL}$ based on its binding kinetics (i.e., binding site concentration, $[\text{nP}] = 3.15 \times 10^{-4} \text{ M}$, and association constant, $K_A = 2.98 \times 10^4 \text{ M}^{-1}$) (29). Hepatic elimination of cefazolin was assumed to be mainly mediated by biliary excretion with an unbound Michaelis-Menten constant $K_{m,u}$ of 163.3 $\mu\text{g/mL}$ (in terms of unbound concentration in liver) and the maximum rate V_{max} of 238.8 $\mu\text{g/min}$, which may reasonably lead to linear excretion kinetics of cefazolin into bile. Therefore, $CL_{u,int}$ (viz., $V_{max}/K_{m,u}$) for biliary excretion was estimated as 1.46 mL/min, and the ER for the well-stirred perfusion-limited liver model (26) calculated with hepatic plasma flow of 3.7 mL/min adopted in Tsuji et al. (1983) (29) was 0.0605 and thus the original $K_{p,ss,Ll}$ was estimated to be 0.740 (Table I). Renal clearance (CL_R) calculated as the slope of the plot of urinary excretion rate versus unbound arterial plasma

concentration of cefazolin divided by f_{up} was 5.03 mL/min. Similarly, the ER for the well-stirred kidney compartment [viz., CL_R/RPF , where renal plasma flow $RPF = 7.3 \text{ mL/min}$ in Tsuji et al. (1983) (29)] led to back estimation of $K_{p,ss}$ for rat kidney to be 0.867 (Table I).

For propranolol, K_p values were reported in Shibasaki et al. (36) after the correction of C_T/C_p values obtained from an IV injection using the traditional C&G method. Using the reported values of R_b (1.16), $f_{up} \cdot CL_{u,int}$ (97.3 mL/min) and Q_{LI} (24.7 mL/min) for liver of a 290-g rat, hepatic ER is estimated as 0.773 (26). Considering the terminal phase slope (0.696 h^{-1}) along with Q_T and V_T values for a 290-g rat, the original C_T/C_p data at 2 h after IV injection were estimated (Table II). In addition, Yata et al. (33) reported propranolol partitioning in liver as $C_{Ll,ss}/C_{out,Ll,ss} = 11.6$ (viz., $C_{out,Ll,ss}$, the outflow plasma concentrations from liver, measured from hepatic vein). However, $K_{p,ss}$ is defined as the tissue-to-‘input’ plasma concentration ratio at steady-state ($C_{Ll,ss}/C_{in,Ll,ss}$ in Eq. 24 for liver). We calculated $K_{p,ss}$ by multiplying $C_{Ll,ss}/C_{out,ss}$ with 0.227 (i.e., $1 - ER$) (Table I). For calculating AUC_T/AUC_p , the tissue concentration profiles of propranolol at 1.5 mg/kg (40) was used since the terminal phase slope (0.66 h^{-1}) was comparable with the literature value (0.696 h^{-1}) at 10 mg/kg (36).

In addition, the steady-state liver-to-plasma concentration ratio was reported for quinidine using the plasma from hepatic portal vein (33). Since it could be assumed that quinidine elimination in rats is mainly mediated by the liver with hepatic blood clearance (CL_H/R_b) of 16.1 mL/min (adjusted by body weight) (37, 48), the ER of quinidine was calculated to be 0.830 (CL_H/Q_{LI}). Therefore, $K_{p,ss}$ was calculated by multiplication of $C_{Ll,ss}/C_{out,Ll,ss}$ (16.5) and $1 - ER$ (0.172) as noted in Table I.

Correction of the Chen and Gross Method Considering f_d

Figures 2a and b exemplify our extension of the C&G method for the theoretical conversion of C_T/C_p to $K_{p,ss}$ using the concentration profiles of furosemide in rat plasma and gut. Using the indicated tri-exponential profile fitted to the observed plasma concentration-time data as a forcing function (i.e., nonlinear regression by the maximum likelihood method in ADAPT 5) (49), tissue distribution parameters (Coefficient of Variation, CV%) for gut were estimated by Eq. 3 with system parameters in Table IV in terms of rate [$f_d = 0.00771$ (16.2%)] and extent [$K_p = 2.61$ (22.0%)]. The observed C_T/C_p was calculated as 10.1 (Table II), which is much higher than the fitted K_p (i.e., model-simulated AUC_T/AUC_p) due to the presence of delayed equilibrium in the early time mediated by both Q_T and $f_{up}PS_{in}$. The calculated f_d values from Models 1 and 2 were 0.0130 and 0.0143, both of which were comparable with the fitted f_d within a factor of

Table III Compound-Specific Input Parameters Used in the Calculations of f_d for Various Tissues of Rats. Sources are Listed in Tables I and II

	Furosemide	Cefazolin	Methotrexate	Etoposide	Dexamethasone	Cyclosporine (low dose) ^a	Cyclosporine (high dose) ^a	Propranolol	Quinidine
f_{up}	0.13 ^b	0.163	0.41 ^b	0.27 ^b	0.175	0.0602	0.0788	0.032	0.4
R_b	0.956	0.55	0.83 ^c	1 ^c	0.725	1.28	1.18	1.16	1.67 ^d
P ^{e,f}	0.013	0.05	0.037	0.33	0.41	2.16	2.16	12	4.2
$f_{up}P/R_b$ ^f	0.00177	0.0148	0.0183	0.0891	0.102	0.0990	0.144	0.331	1.01
Type ^g	Acid	Acid	Zwitterion	Acid	Neutral	Neutral	Neutral	Base	Base
log P	2.03	0.3	-1.85	1.16	1.83	2.9	2.9	3.65	3.44
pKa ₁	4.25	2.3	3.41 (acid)	9.33	-	-	-	9.5	5.4
pKa ₂	9.83	-	2.81 (base)	-	-	-	-	-	10
CL_H (mL/min) ^h	0.259	0.224	1.65	5.40	0.825	0.896	0.826	19.1	26.9
CL_R (mL/min) ^h	0.132	0.820	1.23	0.890	-	-	-	-	-

^aThe values for cyclosporine denote tissue-to-blood partition coefficient at steady-state, with the lower and higher dosages of 2.72 and 13.9 mg/kg/day

^b f_{up} was obtained for furosemide from Yang et al. (41), methotrexate from Berry et al. (42), and etoposide from Yang et al. (43)

^c R_b was obtained for methotrexate from Ueda et al. (44) and etoposide from Nishimura et al. (45)

^dThe data were digitized from the published graph

^eIn vitro PAMPA P coefficients from Kerns et al. (46) except for cefazolin (47)

^fIn vitro PAMPA P and apparent PAMPA P coefficients are presented with units of ($\times 10^{-6}$ cm/s)

^gPhysicochemical properties (log P and pKa) from Jeong et al. (22) for furosemide, methotrexate, and etoposide, Song et al. (27) for dexamethasone, and Rodgers et al. (14, 15) for the others

^hHepatic and renal clearances (with regard to plasma concentration) were calculated from the reported values in the sources listed in Table II, except for methotrexate (30) and etoposide (43)

Table IV System-Specific Input Parameters for 250 g Rat Used for the Conversion of C_T/C_p to $K_{p,ss}$ ^a

	V_T (mL)	Q_T (mL/min)	$S_{eff,Model1}$ (m ² /g tissue)	$S_{eff,Model2}$ (m ² /g tissue)
Adipose	16.7	4.72	3.02	3.30
Bone	15.7	8.08	2.34	2.43
Brain	1.24	1.12	1.67	1.70
Gut	6.19	8.08	16.1	17.9
Heart	1.05	3.2	18.1	19.0
Kidney	2.19	11.6	37.4	39.7
Liver	8.57	19.4	14.8	15.6
Lung	1.24	80	14.4	14.4
Muscle	116	18.96	5.71	7.70
Skin	39.4	4.08	0.843	0.902
Spleen	0.57	0.88	4.56	4.68
Arterial blood	5.11			

^aThe values are consistent with those used in Jeong et al. (22), which are adopted from Simcyp Simulator V15 Release 1 (Simcyp Limited, Sheffield, UK)

2. When f_d was assumed to be 1 (i.e., the C&G method) and 0.130 (e.g., 10-fold of $f_{d,Model1}$), tissue concentration profiles projected from one-time tissue measurement at 8 h (Fig. 2b)

become markedly divergent from the experimental observations. This leads to deviations in K_p estimation (e.g., 9.20 for the C&G method and 7.46 for the case of $10 \times f_{d,Model1}$, compared to the fitted K_p of 2.61).

Based on the assumption of (i) the same terminal slope (β), (ii) gut tissue to be a non-eliminating organ, and (iii) model-dependent f_d values, therefore, $K_{p,ss}$ was estimated from C_T/C_p by Eq. 7, resulting in comparable values (2.53 and 2.72 for Models 1 and 2) with the fitted K_p (i.e., $K_p = K_{p,ss}$ for a non-eliminating organ). However, the experimentally measured $K_{p,ss}$ was 0.517, which is less than the fitted K_p (28). Since this $K_{p,ss}$ was determined after bolus injection of a 25-mg/kg dose followed by a 3-h infusion (11.5 mg/kg/h) and this infusion duration may not be sufficient for the complete equilibrium between plasma and gut (Fig. 2a), one explanation for discrepant $K_{p,ss}$ values between infusion ($C_{T,ss}/C_{p,ss}$) and injection studies (model-simulated AUC_T/AUC_p) could be that a steady-state with regard to gut concentrations might not have been achieved for furosemide by 3 h. Although a steady-state condition is typically confirmed based on serial plasma concentrations, the limited capability in analytical methodologies could have restricted the resolution of all components of drug distribution kinetics specific for those slowly equilibrating tissue(s).

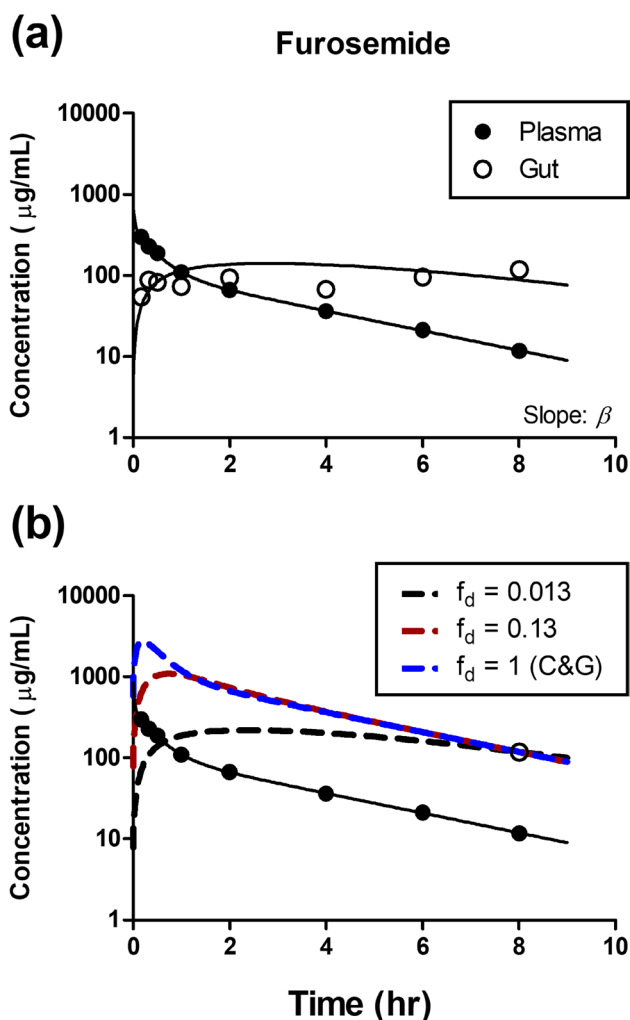


Fig. 2 Concentration profiles of furosemide in rat plasma (closed circles) and gut (open circles). (a) Solid lines show fittings to the concentration-time data in the plasma ($C_p = 455.3 \cdot e^{-40.2 \cdot t} + 287 \cdot e^{-2.42 \cdot t} + 113 \cdot e^{-0.282 \cdot t}$) and gut (f_d and K_p optimized by Eq. 3 with C_p used as a forcing function; see text). (b) For the case of one-time measurement of tissue concentration at 8 h, dashed lines show tissue concentration profiles assumed in determination of $K_{p,ss}$ (or AUC_T/AUC_p) depending on f_d values (e.g., 0.0130 from Model 1 and 1 from the C&G method)

As shown in Fig. 3, tissue partition coefficients (C_T/C_p and $K_{p,ss}$ from different approaches) collected for 8 compounds in various tissues of rats ranged about 4 orders of magnitude. When C_T/C_p is directly compared with $K_{p,ss}$ for the 8 compounds, 69 out of 74 points showed C_T/C_p values larger than $K_{p,ss}$, supporting the contribution of an equilibrium time between plasma and tissues emerging in the terminal phase after bolus dosing (Fig. 3a). For furosemide having the lowest permeability coefficient amongst our assessed compounds, $K_{p,ss}$ for gut was obviously different than C_T/C_p (19.5-fold). For quinidine, the highest

permeability drug, $K_{p,ss}$ for liver was different from C_T/C_p (14.7-fold). As shown in Fig. 3b, however, the $K_{p,ss}$ estimated with the C&G method employing the same terminal slope (β) and $R_b = 1$ appears to have comparable values with the uncorrected C_T/C_p . Since the C&G method does not consider a tissue permeability term $f_{up}PS_{in}$, the $K_{p,ss}$ estimation based on the traditional method is expected to be problematic for drugs having lower permeability coefficients.

In our extensions of the C&G approach, a compound-specific R_b was utilized (Table III), and tissue-specific slopes were considered where the tissue kinetic profiles were found for furosemide, cefazolin, cyclosporine, and quinidine as listed in Table II. Otherwise, all the profiles in tissues and plasma/blood were assumed to decline in parallel, using Eqs. 7, 13, 20 and 27. However, Fig. S1 shows that consideration of different slopes (β_T) for the 4 drugs in the calculation of $K_{p,ss}$ from C_T/C_p was not significantly different than using the same slope (β). When f_d values for Models 1 and 2 (Figs. 3c and d) were calculated for the 8 compounds in the major tissues of rats, our estimations of $K_{p,ss}$ were improved particularly for the lower permeability compound, viz., furosemide. The coefficients of determination (R^2) for Fig. 3a to d for the 4 different methods are very close: 0.9104 (C_T/C_p), 0.9102 (C&G), 0.9184 (Model 1), and 0.9173 (Model 2).

As shown in Fig. 4, the predicted $K_{p,ss}$ (i.e., 4 in silico approaches plus 4 different experimentally-based approaches) and in vivo $K_{p,ss}$ values are plotted in terms of fold-differences ($K_{p,ss,pred}/K_{p,ss}$). In agreement with the regressions shown in Fig. 3, the four versions of the C&G calculations produce K_p ratios near unity (Fig. S2) and the acceptable predictability was shown with Models 1 and 2 (i.e., the fold-differences closer to 1). While the improvements of $K_{p,ss}$ predictions in many different types of tissues for furosemide (gut), cefazolin (kidney and skin), etoposide (gut, muscle, and spleen), and propranolol (brain and lung) supports the usefulness of the extended C&G method, some overpredictions in $K_{p,ss,pred}/K_{p,ss}$ remained unimproved despite the current f_d considerations. There appeared to be no consistency when comparing specific tissues. Very striking in Fig. 4 are the disparate K_p ratios observed with the four in silico estimation methods. Of note, the experimental ER values calculated as the ratios of $CL_H/(Q_{LT}R_b)$ and $CL_R/(Q_{KT}R_b)$ are less than the model-dependent f_d values, or comparable with f_d (within a factor of 2). When $ER > f_d$, the in silico K_p was not further converted to $K_{p,ss}$ for furosemide and methotrexate (liver and kidney), cefazolin (kidney), and propranolol (liver). In general, these in silico methods for the 8 compounds assessed function poorly for predicting $K_{p,ss}$ (Fig. 4), compared to the experimental AUC_T/AUC_p or C_T/C_p values (i.e., $K_{p,ss,pred}/K_{p,ss}$ closer to 1). The greatest mis-predictions occurred with the liver, especially for high ER drugs, viz., propranolol and quinidine.

Discussion

The classic drug-specific components of PBPK models are the clearance (e.g., $CL_{u,int}$) and the operative tissue-partition (K_p) parameters that, along with system components such as Q_T and V_T , serve in the simplest of PBPK models. The gold-standard approach to assessing both clearances and K_p values is a steady-state infusion study. The second-most common method is to enact single-dose studies to assess (systemic) clearance from $Dose/AUC$ and K_p from AUC_T/AUC_p . The limitation of this method, even by performing computational fitting, is that an IV bolus study often assumes an initial condition $C_p(0)$ of $Dose/V_B$ or $Dose/V_p$, which may not be supported by sufficient early blood samples. All experimental methods have concerns when metabolism, permeability, or transporters affect the measured tissue drug concentration. The terminal phase in a pharmacokinetic profile, if not limited by assay sensitivity, often has the richest data and can be visualized with both plasma (blood) and tissue measurements, which prompted the derivation of the C&G method for calculating K_p . This method has been widely used with 166 citations based on a Google Scholar search (last accessed 28 Jan 2022).

In line with Eq. 1, a typical PBPK equation for a perfusion-limited tissue compartment (eliminating organ) is written as:

$$V_T \frac{dC_T}{dt} = Q_T \cdot R_b \cdot \left(C_p - \frac{C_T}{K_p} \right) - CL_{u,int} \cdot f_{up} \cdot \frac{C_T}{K_p} \quad (34)$$

where C_T/K_p denotes C_{out} under the assumption of symmetrical transport. Therefore, when the perfusion-limited model is assumed for non-eliminating (Eq. 1) and eliminating organs (Eq. 34) with $PS_{in} = PS_{out}$, a ‘PBPK-applicable’ K_p (viz., f_{up}/f_{uT} in this case) could be obtained from the direct measurement of C_T/C_{out} , as attempted for propranolol and quinidine in rat liver (33). However, since measurement of C_{out} from general tissues is experimentally difficult, investigators mostly take advantage of using C_{in} (e.g., arterial concentration), which is widely used to determine $K_{p,ss}$ in experimental animal species. However, if significant elimination occurs in particular tissues, C_{out} will be smaller than C_{in} , and ER determined by the organ clearance divided by blood flow (e.g., CL_H/Q_{LT}) can be used for the conversion of $K_{p,ss}$ to K_p . Based on perfusion-limited distribution kinetics, ER could be calculated in another way by using $CL_{u,int}$ and Q_{LT} depending on the clearance models. Recently, we reviewed the usefulness of classical hepatic clearance models such as well-stirred model (WSM), parallel tube model (PTM), and dispersion model (DM) (50), which have different kinetic characteristics in terms of elimination clearance leading to the model-dependent estimates of $CL_{u,int}$ to achieve the same systemic exposure. These clearance models are based on

the same unbound concentration between plasma and liver (e.g., $C_{u,LI} = C_{up} = f_{up} C_{out}$ for WSM), which is the driving concentration of hepatic elimination. Therefore, it is worth noting that, since the total liver concentration is instantaneously equilibrated with plasma (e.g., $C_{LI} = K_{p,LI} C_{out}$ for WSM), all these models assume well-mixed kinetics with regard to drug distribution to liver (i.e., no diffusion barrier). Accordingly, the relationship of $K_p = C_T/C_{out}$ in traditional clearance models is useful for eliminating organs (Eq. 34) as applied for non-eliminating organs (Eq. 1), but only for compounds following perfusion-limited distribution kinetics. As noted in the previous literature (19) regarding elimination in peripheral tissues without a permeability limitation, the conversion of $K_{p,ss}$ to K_p by the C&G method is based on the well-stirred and perfusion-limited distribution model (21).

However, the following conditions violate Eq. 34: First, asymmetric transport (i.e., $PS_{in} \neq PS_{out}$). Active transport mediated by membrane transporters (17) and/or electrogenic transport driven by membrane potential (51) could lead to different unbound concentrations between plasma and tissue cells. In this case, C_{up} would not be adequate for describing the driving force concentration in tissue, since C_{uT} , which would be effectively acting upon the metabolism / excretion by enzymes / transporters inside the cells, is now different from C_{up} . For asymmetric transport, therefore, Eq. 28 should be considered. If the use of Eq. 34 is still applicable even when asymmetric transport between plasma and tissue cells is involved with the eliminating organ, employing C_{up} as the driving force concentration in such conditions should be discussed and rationalized.

Secondly, a limitation in tissue permeability (i.e., $f_{up} PS_{in}/R_b \ll Q_T$) necessitates the use of Eq. 8. For a non-eliminating organ, the steady-state condition leads to the relationship of $K_p = K_{p,ss}$ regardless of whether f_d is considered in Eq. 1 or not. For an eliminating organ, however, Eq. 8 shows that the term f_d needs to be present in the mathematical relationship between K_p and $K_{p,ss}$ at steady-state. Eq. 30 was derived showing that traditional conversion of $K_{p,ss}$ to K_p (19) would not be valid for the case of $f_d \neq 1$. For imipramine, propranolol, and quinidine, the concentration ratio between liver and plasma in the hepatic vein ($C_{LI,ss}/C_{out,ss}$) observed in the literature (33) was reported as K_p , probably based on perfusion-limited distribution kinetics. For propranolol, the model-dependent f_d for liver was calculated to be 0.728 and 0.578 for Models 1 and 2, which are comparable with the ER (0.773), suggesting that $PS_{out} \ll CL_{u,int}$ (see Eq. A4 in the APPENDIX). For quinidine, f_d values for liver in Models 1 and 2 were estimated as 0.981 and 0.807, also suggesting sufficient tissue permeability. However, if a significant limitation in tissue permeability is evident (i.e., $f_{up} PS_{in}/R_b \ll Q_T$ or $f_d \ll 1$), $C_{LI,ss}/C_{out,ss}$ would not represent K_p .

Fig. 3 Estimation of $K_{p,ss}$ (a) from direct comparison with C_T/C_p (Table II), converted from (b) traditional Chen and Gross (C&G) method (i.e., $R_b=1$ and the same terminal slope), and revised methods with (c) Model 1 and (d) Model 2. Solid line has a slope of 1.0, and dashed lines show 3-fold differences

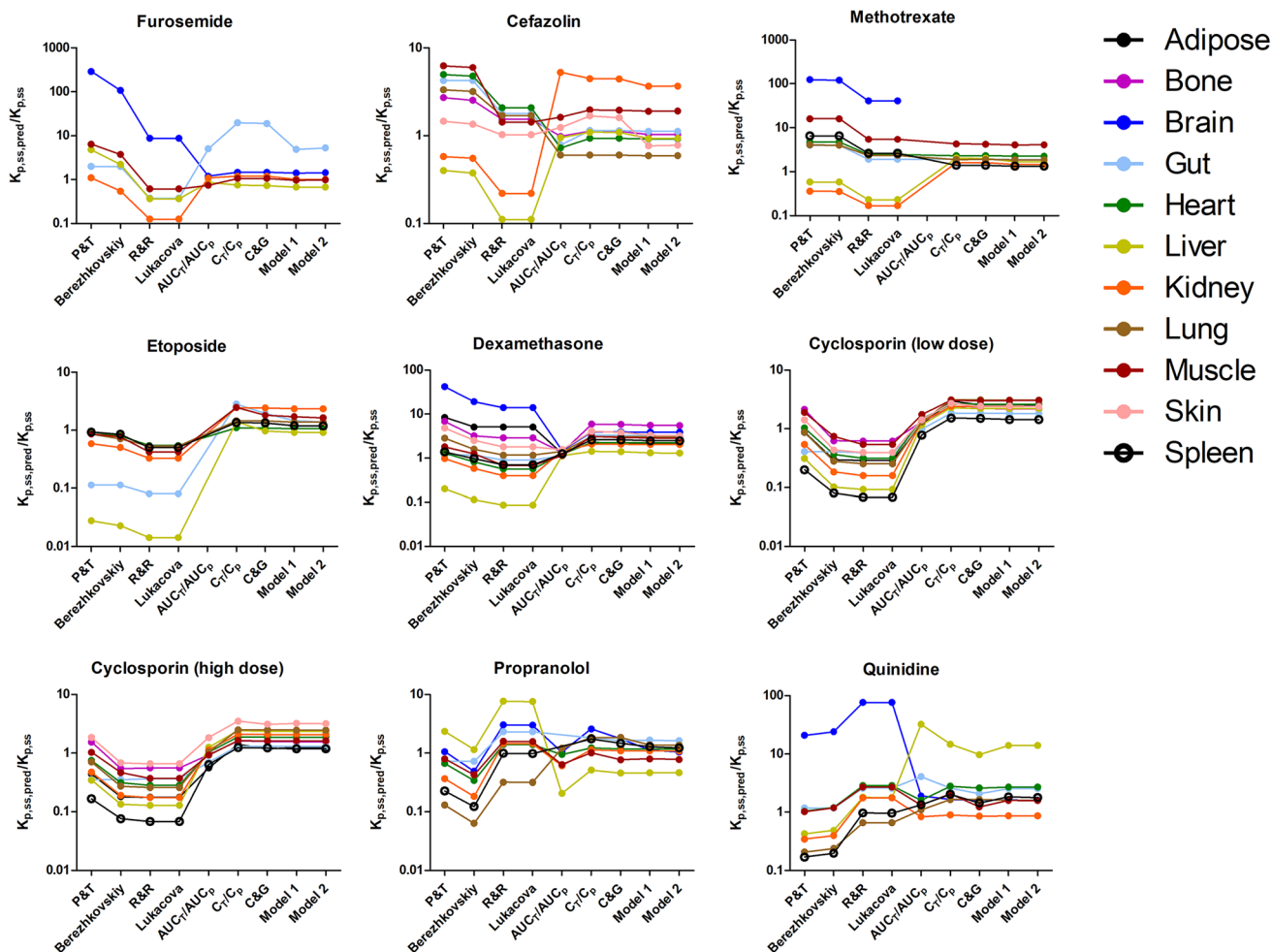
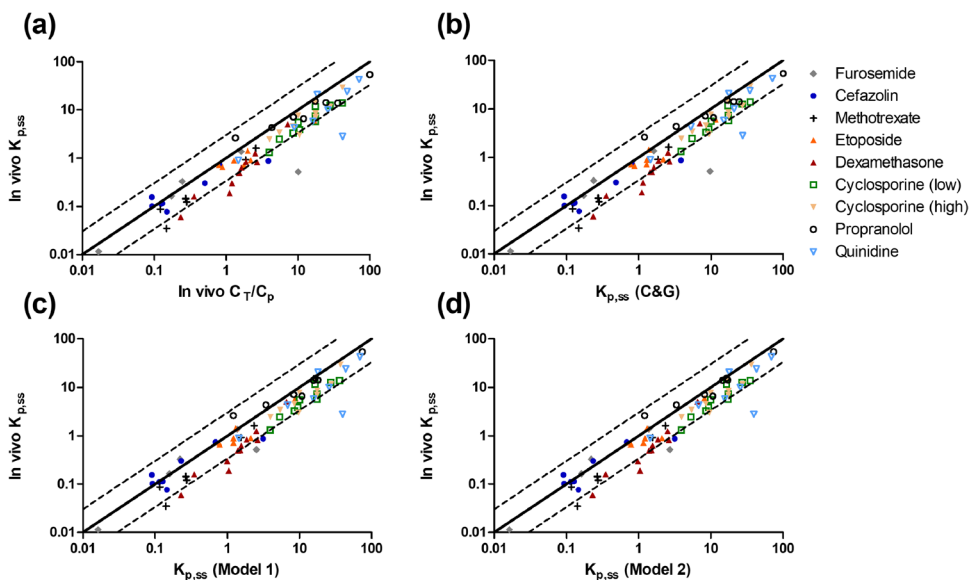


Fig. 4 Comparisons of $K_{p,ss}$ with (i) AUC_T/AUC_p , (ii) C_T/C_p , and $K_{p,ss}$ calculated from (iii) the Chen and Gross method (C&G), (iv) Model 1, and (v) Model 2, for 8 compounds assessed. The in silico calculations employed the Poulin and Theil (P&T) (11, 12), Berezhtkovskiy (13), Rodgers and Rowland (R&R) (14, 15), and Lukacova (16) methods. The Y-axis denotes the predictability of each method ($K_{p,ss,pred}/K_{p,ss}$) and dots are connected to visualize the specific tissues

In addition, Eq. A4 derived for ER is consistent with the extended clearance model that factors membrane transport into the elimination kinetics (18, 52). Thus, kinetic interpretation of ER determined by $(C_{in} - C_{out})/C_{in}$ would be reasonable with Eq. A4 when membrane transport takes part in the elimination process. In terms of distribution kinetics, however, Eq. 30 shows that the traditional relationship [i.e., $K_{p,ss} = K_p \cdot (1 - ER)$] (19) is not always the case. When Eq. A2 is derived based on distribution Model 2, this traditional relationship would operate properly only when $PS_{out} \gg CL_{u,int}$. For the case of $PS_{out} \ll CL_{u,int}$, ER determined by using C_{in} and C_{out} from an isolated liver perfusion study would appear to be representative of, or limited by, f_d (Eq. A4). Since furosemide is a substrate of organic anion transporting polypeptide 2B1 (OATP2B1) (53) and organ anion transporters (OATs) (54–56) and cefazolin is a substrate of OAT3 (57), the inclusions of these active uptake kinetics in PS_{in} of Eqs. 33a and 33b for liver and/or kidney would lead to improved predictions of f_d and thus the relationship $ER < f_d$. Of note, the previous review of the extended clearance concept (18) reported the general K_p equation as $f_{up}PS_{in}/(f_{uT}(PS_{out} + CL_{u,int}))$, which seems to satisfy the traditional relationship (19). However, the ‘true’ K_p that is applicable for PBPK equations should be expressed in accordance with Eq. 2, which is independent of the elimination kinetic variable, $CL_{u,int}$.

Collectively, therefore, the traditional C&G method that facilitates conversion of C_T/C_p from a bolus injection to the PBPK-applicable K_p appears problematic when $f_d \ll 1$ in terms of two aspects: f_d involvements (i) from C_T/C_p to $K_{p,ss}$ (Eqs. 7 and 13), and (ii) from $K_{p,ss}$ to K_p for eliminating organs (Eq. 30). Compared to the traditional C&G method, our extension considering f_d shows considerable improvement when $K_{p,ss}$ was estimated from C_T/C_p particularly for furosemide (Figs. 3c and d), the compound with the lowest apparent PAMPA P coefficient (Table III). We also included the blood partitioning property (R_b) in the original C&G relationship, as expanded in Shibasaki et al. (36). Tissue concentration-time profiles were available for furosemide (28), cefazolin (29), cyclosporine (34), and quinidine (37), showing that the terminal phase slope could be different depending on tissues. When linear pharmacokinetics applies, terminal phase slopes for all biological tissue matrices should become the same (20), which is the major kinetic basis considered in the C&G method. However, if terminal phases are evidently different and a limitation in analytical methodology hinders the determination of lower concentrations sufficient to experimentally prove the parallel decline, Eqs. 31a to 31c could be useful for $K_{p,ss}$ estimation.

The parameter $K_{p,LU}$ denotes the lung-to-‘venous’ plasma partition coefficient, and Eq. 20 enables the theoretical estimation of $K_{p,LU}$ from bolus dose studies when arterial C_p is determined instead of $C_{ven,p}$, which should

be the theoretically complete mixture of outflow concentrations from various tissues and would be experimentally difficult to measure. Levitt (58) provided site-dependent plasma concentration-time profiles for ethanol, thiopental, Tc-99 m-diethylene triamine pentaacetate, and ketamine, dosed in humans (e.g., blood collected from antecubital vein and artery). For these drugs, arterial concentrations were higher than venous concentrations especially in the early phase after drug administration, both of which became comparable later in time. In a poly-exponential disposition curve, the apparent slope could be expressed as $\beta_{app}(t)$. Since $\beta_{app}(t)$ in lung and arterial plasma (i.e., for short term infusion, an upcurve resulting from negative coefficient) would be mainly governed by steeper slopes (or larger positive eigenvalues) in the early phase after drug dosing, the application of $\beta_{app}(t)$ in the term β of left-hand sides of Eqs. 18 and 19a would result in the early-phase discrepancy between $C_{ven,p}$ and $C_{out,LU}$ (normalized by C_{LU}) and between $C_{out,LU}$ and C_p (normalized by C_p) where $C_p \gg C_{ven,p}$. With the passage of time, however, a more shallow slope emerging with transit times such as V_{LU}/Q_{LU} (e.g., 0.0155 min for rat, and 1170/5600 = 0.209 min for man) and V_{art}/Q_{LU} (0.0639 min for rat and 1730/5600 = 0.310 min for man) (25) leads to insignificant differences between $C_{ven,p}$ and C_p , as observed with the 4 drugs above.

The physical meaning of Eqs. 7 and 13 for typical tissues is that an instantaneous equilibrium between C_T and C_p may not be physically possible due to the presence of a distribution rate process such as Q_T and $f_{up}PS_{in}$, and thus C_T/C_p could be significantly larger than $K_{p,ss}$ (Fig. 3a). The relative error of C_T/C_p for estimation of $K_{p,ss}$ can be calculated by rearrangement of Eqs. 7 and 13 as:

$$\frac{C_T/C_p - K_{p,ss}}{K_{p,ss}} = \frac{V_T \beta}{Q_T f_d R_b} \cdot \frac{C_T}{C_p} \quad (35)$$

Therefore, the direct consideration of C_T/C_p , which is frequently reported as the apparent tissue-to-plasma partition coefficient, as $K_{p,ss}$ may be less problematic for the cases (i) with a sufficiently long half-life, (ii) high tissue permeability coefficient (higher f_d), (iii) highly perfused organs (low V_T/Q_T), and (iv) low C_T/C_p value itself. Theoretically, steady-state $K_{p,ss}$ can be determined by measurements of $C_{T,ss}$ and $C_{p,ss}$ after infusion as well as AUC_T and AUC_p after a bolus injection. Thus, when early-time tissue data are not sufficient to adequately determine $K_{p,ss} = AUC_T/AUC_p$, our theoretical relationships would be also useful for $K_{p,ss}$ estimation from even a one-time observation of C_T/C_p .

Linear pharmacokinetic theories feature the same eigenvalues (or slopes) for disposition functions regardless of route of administration (e.g., oral, subcutaneous, intramuscular, etc.). However, slow absorption rates lead to addition of a late exponential phase with the slope representing

the absorption rate constant k_a (i.e., first-order absorption under linear kinetics). For the case of k_a faster than β , Eqs. 7, 13, 20, and 27 would be still applicable. For flip-flop kinetics ($k_a \ll \beta$), post-distributive concentration profiles would decline in parallel with the slope of k_a that takes the role of terminal phase slope β in the above four equations.

While the derived extensions of the C&G method proved advantageous for only 1 of 8 compounds where K_p was measured by several methods in rats, our methodology provides new insights into the role of tissue permeability in PBPK models and has the potential to be relevant to numerous additional drugs. For example, most of the compounds (22 out of 24) administered to rats assessed in Jeong et al. (22) are expected to have permeability-limited distribution kinetics whose contribution appears in the plasma concentration profiles (i.e., $f_{up}PS_{in} < 1.0 \times 10^{-6}$ cm/s). When Benet (59) examined 698 drugs on the market and 28,912 new molecular entities (NMEs), 27% of the marketed drugs and 28% of NMEs fall into the BDDCS low-permeability categories 3 and 4. Since the contribution of active transport mechanisms to the overall permeability across the biological membranes of tissues could become dominant for such low permeability compounds (60), caution is needed in assuming perfusion-limited distribution and trusting in silico methods of estimating K_p values for such cases when performing top-down PBPK modeling.

The current approach and applications extending the C&G method have some limitations. Firstly, only 8 compounds were assessed owing to the few drugs studied where tissue distribution data were available from both steady-state infusions and single-dose bolus studies in rats. Non-linear pharmacokinetics could result in potential discrepancies. From the literature (37), nonlinear binding of quinidine in rat blood was observed, and f_{up} and R_b (Table III) reflect a saturable plasma concentration at 6 $\mu\text{g/mL}$ with an $f_{up}P/R_b$ value of 1.01×10^{-6} cm/s. However, a lower plasma concentration (0.455 $\mu\text{g/mL}$) of quinidine with different values of f_{up} (0.25) and R_b (1.1) had a $f_{up}P/R_b$ value of 0.955×10^{-6} cm/s. More dramatic differences in f_{up} depending on the concentration were observed for furosemide from 0.00716 to 0.0224 (10 to 250 $\mu\text{g/mL}$) (28), which could be variable up to 0.13 (at 10 $\mu\text{g/mL}$) (41). If a concentration decay leads to $f_{up}P/R_b$ changing from above to below the threshold condition of $f_{up}P/R_b = 1 \times 10^{-6}$ cm/s proposed for perfusion-limited distribution kinetics (22), the whole-body PBPK model structure should be able to operate with the perfusion-limited kinetics in the initial phase with higher concentrations, followed by permeability-limited kinetics in the later phase with lower concentrations. Nevertheless, the consideration of a potentially saturable f_{up} for furosemide was useful for reasonable correction of C_T/C_p to $K_{p,ss}$ (Figs. 3c and d). Kitani et al. (28) showed furosemide concentrations in gut (C_{GU}) that were consistently around 100 $\mu\text{g/mL}$ when

plotted against free concentrations in plasma (C_{up}) from 0.1 to 10 $\mu\text{g/mL}$, suggesting a possibility of saturated binding properties in the C_{up} range ($[nP] \ll C_{up}$). However, this interpretation would need further refinement since instantaneous equilibrium between C_{up} and C_{iT} may not be achieved for furosemide due to its low permeability. For methotrexate, non-linear distribution to liver, kidney, and bone marrow of rats was evident with increased C_T/C_p over time (61). Quinidine was suggested to be distributed into rat liver in a concentration-dependent manner, resulting in a liver-specific β_{LI} (37). When non-linear kinetics is evident, however, the application of β_{LI} in Eq. 31c may be problematic. For quinidine, Eq. 31c was not sufficient for more reliable estimation of $K_{p,ss}$ compared to the C&G method since the perfusion-limited liver model would be applicable based on f_d values close to 1 (e.g., 0.981 and 0.807 for Models 1 and 2).

In line with this, the majority of the data points with C_T/C_p values larger than $K_{p,ss}$ found in Fig. 3a supports the contribution of an equilibrium process between plasma and tissues after bolus dosing, while many of the points remain under the unity line in Figs. 3c and d even with our consideration of f_d in the C&G method. When the plasma (blood for dexamethasone and cyclosporine) concentrations ($\mu\text{g/mL}$) measured for the calculations of C_T/C_p and $K_{p,ss}$ are collected for furosemide (11.7 and 111), cefazolin (84.5 and 77.5), methotrexate (3.11 and 11.1), etoposide (1.3 and 15.9), dexamethasone (0.00145 and 0.355), cyclosporine (0.2 and 0.49/2.7), propranolol (0.501 and 0.830), and quinidine (0.763 and 0.843), the values from bolus studies are smaller than, or comparable, with steady-state values. If non-linear kinetics are involved with tissue binding and/or uptake processes (e.g., driven by plasma concentration), then lower plasma concentrations after bolus injections may lead to C_T/C_p -derived estimates that are generally higher than $K_{p,ss}$. In addition, the t_{last} for determining C_T/C_p would need to be long enough to ensure the parallel decline between plasma and tissues. In rats, the terminal phase half-life of etoposide at $t_{last} = 1$ h was 20 min (31) whereas the half-life at $t_{last} = 8$ h was 110 min (62). Thus, determination of C_T/C_p for etoposide at a later phase would reflect more complete achievement of equilibrium between plasma and tissues. For compounds having time-dependent (rather than rapid) distribution into red blood cells as shown for tacrolimus (63) and metformin (64), it would be necessary to use the equilibrated R_b value in Eqs. 7, 13, 20, and 27 derived in this study.

Conclusions

Over time, many complexities have been encountered in pharmacokinetics and application of PBPK models. These include the involvement of plasma and tissue drug

binding, red blood cell distribution, permeability-limited tissue uptake, transporters, alternative organ models, and others (50). Since determinations of tissue concentrations at different times are labor-intensive and time-consuming when assessing many different tissues, the C&G method was derived to enhance the practical utility of a one-time measurement of C_T/C_p in the terminal phase. However, it is evident that the perfusion-limited distribution is not always the case in PBPK models (22) and thus this report primarily addresses our extension of the C&G method for the extent of tissue distribution (e.g., C_T/C_p and $K_{p,ss}$) that are theoretically associated with the distribution rates (e.g., Q_T and $f_{up}PS_{in}$). We herein included the fractional distribution parameter f_d , which readily enables considerations of membrane permeability limitations in the rate of tissue distribution, into the traditional C&G concept. The theoretical relationship between C_T/C_p and $K_{p,ss}$ was derived for typical non-eliminating (Eq. 3), eliminating tissues (Eq. 4), lung (Eq. 20), and liver (Eq. 27). When different terminal slopes are obtained, a tissue-specific β_T can be applied based on a linear kinetic assumption. We demonstrated the theoretical conversion of C_T/C_p to $K_{p,ss}$ measured for 8 compounds with a wide range of apparent PAMPA P coefficients. For conversion of $K_{p,ss}$ to the PBPK-applicable K_p for eliminating organs, we showed that the traditional correction method utilizing ER would not be valid when $f_d \ll 1$. When more realistic f_d values are considered along with the inclusions of a passive component of tissue permeability, the current extension of the C&G method should increase the utility of interpreting tissue-plasma concentration ratios in PBPK. Lastly, while the use of 8 compounds represents a limited database, it is noteworthy that none of the four in silico methods performed well with a considerable spread of K_p ratios among the up to 11 tissue types. It should be kept in mind that published graphs showing concordance of calculated versus measured K_p values feature data from diverse drugs and tissues in log-log plots where discrepancies are obscured by such a wide scaling of data. Predictability should be considered as only approximate with limited confirmation possible by calculation of in vivo V_{SS} values.

Appendix

Eq. 8, which is another expression of Eq. 28, can be rewritten for a steady-state condition by considering C_p as the input concentration as:

$$Q_T f_d R_b \cdot \left(1 - \frac{C_{T,ss}/C_{in,ss}}{K_p}\right) - CL_{u,int} f_{uT} \cdot \frac{C_{T,ss}}{C_{in,ss}} = 0 \quad (A1a)$$

$$K_{p,ss} = \frac{C_{T,ss}}{C_{in,ss}} = \frac{Q_T f_d R_b K_p}{Q_T f_d R_b + CL_{u,int} f_{uT} K_p} \quad (A1b)$$

In addition, Model 2 is structurally the same with the extended clearance model for membrane-limited transport (18, 52). Substitution of Eq. 33b into Eq. A1b leads to:

$$K_{p,ss} = \frac{PS_{out}}{PS_{out} + CL_{u,int}} \cdot \frac{Q_T R_b}{Q_T R_b + f_{up} PS_{in}} \cdot \frac{CL_{u,int}}{PS_{out} + CL_{u,int}} \cdot K_p \quad (A2)$$

From Eq. 28, a steady-state condition leads to the following relationship for a traditional organ extraction ratio (ER):

$$ER = \frac{C_{in,ss} - C_{out,ss}}{C_{in,ss}} = \frac{CL_{u,int} f_{uT}}{Q_T R_b} \cdot \frac{C_{T,ss}}{C_{in,ss}} = \frac{CL_{u,int} f_{uT}}{Q_T R_b} K_{p,ss} \quad (A3)$$

Expanding Eq. A3 for Model 2 with Eq. A2 can be considered as:

$$ER = \frac{f_{up} PS_{in} \cdot \frac{CL_{u,int}}{PS_{out} + CL_{u,int}}}{Q_T R_b + f_{up} PS_{in} \cdot \frac{CL_{u,int}}{PS_{out} + CL_{u,int}}} < \frac{f_{up} PS_{in}}{Q_T R_b + f_{up} PS_{in}} = f_{d,Model2} \quad (A4)$$

which is consistent with the previous literature (18, 52) for hepatic clearance as the product of the plasma flow ($Q_T R_b$) and ER in Eq. A4.

Supplementary Information The online version contains supplementary material available at <https://doi.org/10.1007/s11095-022-03211-3>.

Acknowledgments and Disclosures This research was supported by the NIH Grant R35 GM131800. The authors have declared that there is no conflict of interest.

References

1. Gillette JR. Factors affecting drug metabolism. *Ann N Y Acad Sci.* 1971;179(1):43–66.
2. Wilkinson GR, Shand DG. A physiological approach to hepatic drug clearance. *Clin Pharmacol Ther.* 1975;18(4):377–90.
3. Øie S, Tozer TN. Effect of altered plasma protein binding on apparent volume of distribution. *J Pharm Sci.* 1979;68(9):1203–5.
4. Rowland M, Benet LZ, Graham GG. Clearance concepts in pharmacokinetics. *J Pharmacokinet Biopharm.* 1973;1(2):123–36.
5. Gibaldi M, Perrier D. *Pharmacokinetics*. 2nd ed. New York: M. Dekker; 1982. p. 355–64.
6. Mendel CM. The free hormone hypothesis: a physiologically based mathematical model. *Endocr Rev.* 1989;10(3):232–74.
7. Lin JH. Tissue distribution and pharmacodynamics: a complicated relationship. *Curr Drug Metab.* 2006;7(1):39–65.
8. Kalvass CJ, Maurer TS. Influence of nonspecific brain and plasma binding on CNS exposure: implications for rational drug discovery. *Biopharm Drug Dispos.* 2002;23(8):327–38.

9. Jusko WJ, Molins EA, Ayyar VS. Seeking nonspecific binding: assessing the reliability of tissue dilutions for calculating fraction unbound. *Drug Metab Dispos.* 2020;48(10):894–902.
10. Berry LM, Roberts J, Be X, Zhao Z, Lin MH. Prediction of V_{ss} from in vitro tissue-binding studies. *Drug Metab Dispos.* 2010;38(1):115–21.
11. Poulin P, Theil FP. Prediction of pharmacokinetics prior to in vivo studies. I. Mechanism-based prediction of volume of distribution. *J Pharm Sci.* 2002;91(1):129–56.
12. Poulin P, Theil FP. Prediction of pharmacokinetics prior to in vivo studies. II. Generic physiologically based pharmacokinetic models of drug disposition. *J Pharm Sci.* 2002;91(5):1358–70.
13. Berezhkovskiy LM. Volume of distribution at steady state for a linear pharmacokinetic system with peripheral elimination. *J Pharm Sci.* 2004;93(6):1628–40.
14. Rodgers T, Leahy D, Rowland M. Physiologically based pharmacokinetic modeling 1: predicting the tissue distribution of moderate-to-strong bases. *J Pharm Sci.* 2005;94(6):1259–76.
15. Rodgers T, Rowland M. Physiologically based pharmacokinetic modelling 2: predicting the tissue distribution of acids, very weak bases, neutrals and zwitterions. *J Pharm Sci.* 2006;95(6):1238–57.
16. Lukacova V, Parrott NJ, Lavè T, Fraczkiewicz G, Bolger MB, Woltosz WS. Role of fraction unbound in plasma in calculation of tissue:plasma partition coefficients. Atlanta: AAPS National Meeting; 2008.
17. Shitara Y, Horie T, Sugiyama Y. Transporters as a determinant of drug clearance and tissue distribution. *Eur J Pharm Sci.* 2006;27(5):425–46.
18. Shitara Y, Maeda K, Ikejiri K, Yoshida K, Horie T, Sugiyama Y. Clinical significance of organic anion transporting polypeptides (OATPs) in drug disposition: their roles in hepatic clearance and intestinal absorption. *Biopharm Drug Dispos.* 2013;34(1):45–78.
19. Berezhkovskiy LM. A valid equation for the well-stirred perfusion limited physiologically based pharmacokinetic model that consistently accounts for the blood–tissue drug distribution in the organ and the corresponding valid equation for the steady state volume of distribution. *J Pharm Sci.* 2010;99(1):475–85.
20. Vaughan DP, Dennis MJ. Number of exponential terms describing the solution of an N-compartmental mammillary model: vanishing exponentials. *J Pharmacokin Biopharm.* 1979;7(5):511–25.
21. Chen HSG, Gross JF. Estimation of tissue-to-plasma partition coefficients used in physiological pharmacokinetic models. *J Pharmacokin Biopharm.* 1979;7(1):117–25.
22. Jeong Y-S, Yim C-S, Ryu H-M, Noh C-K, Song Y-K, Chung S-J. Estimation of the minimum permeability coefficient in rats for perfusion-limited tissue distribution in whole-body physiologically-based pharmacokinetics. *Eur J Pharm Biopharm.* 2017;115:1–17.
23. Thompson MD, Beard DA. Development of appropriate equations for physiologically based pharmacokinetic modeling of permeability-limited and flow-limited transport. *J Pharmacokin Pharmacodyn.* 2011;38(4):405–21.
24. Cao Y, Jusko WJ. Applications of minimal physiologically-based pharmacokinetic models. *J Pharmacokin Pharmacodyn.* 2012;39(6):711–23.
25. Davies B, Morris T. Physiological parameters in laboratory animals and humans. *Pharm Res.* 1993;10(7):1093–5.
26. Pang KS, Rowland M. Hepatic clearance of drugs. I. Theoretical considerations of a “well-stirred” model and a “parallel tube” model. Influence of hepatic blood flow, plasma and blood cell binding, and the hepatocellular enzymatic activity on hepatic drug clearance. *J Pharmacokin Biopharm.* 1977;5(6):625–53.
27. Song D, Sun L, DuBois DC, Almon RR, Meng S, Jusko WJ. Physiologically based pharmacokinetics of dexamethasone in rats. *Drug Metab Dispos.* 2020;48(9):811–8.
28. Kitani M, Ozaki Y, Kitayama K, Kakemi M, Koizumi T. A kinetic study on drug distribution: furosemide in rats. *Chem Pharm Bull.* 1988;36(3):1053–62.
29. Tsuji A, Yoshikawa T, Nishide K, Minami H, Kimura M, Nakashima E, et al. Physiologically based pharmacokinetic model for β -lactam antibiotics I: tissue distribution and elimination in rats. *J Pharm Sci.* 1983;72(11):1239–52.
30. Yokooji T, Mori N, Murakami T. Modulated pharmacokinetics and increased small intestinal toxicity of methotrexate in bilirubin-treated rats. *J Pharm Pharmacol.* 2011;63(2):206–13.
31. Carcel-Trullols J, Torres-Molina F, Araico A, Saadeddin A, Peris JE. Effect of cyclosporine a on the tissue distribution and pharmacokinetics of etoposide. *Cancer Chemother Pharmacol.* 2004;54(2):153–60.
32. Bernareggi A, Rowland M. Physiologic modeling of cyclosporin kinetics in rat and man. *J Pharmacokin Biopharm.* 1991;19(1):21–50.
33. Yata N, Toyoda T, Murakami T, Nishiura A, Higashi Y. Phosphatidylserine as a determinant for the tissue distribution of weakly basic drugs in rats. *Pharm Res.* 1990;7(10):1019–25.
34. Kawai R, Mathew D, Tanaka C, Rowland M. Physiologically based pharmacokinetics of cyclosporine a: extension to tissue distribution kinetics in rats and scale-up to human. *J Pharmacol Exp Ther.* 1998;287(2):457–68.
35. Park JM, Ahn BN, Yoon EJ, Lee MG, Shim CK, Kim CK. The pharmacokinetics of methotrexate after intravenous administration of methotrexate-loaded proliposomes to rats. *Biopharm Drug Dispos.* 1994;15(5):391–407.
36. Shibasaki S, Asahina M, Kawamata Y, Kojo M, Nishigaki R, Umemura K. The inhibitory effects of cimetidine on elimination and distribution of propranolol in rats. *J Pharmacobio-Dyn.* 1989;12(9):549–57.
37. Harashima H, Sawada Y, Sugiyama Y, Iga T, Hanano M. Analysis of nonlinear tissue distribution of quinidine in rats by physiologically based pharmacokinetics. *J Pharmacokin Biopharm.* 1985;13(4):425–40.
38. Kety SS. The theory and applications of the exchange of inert gas at the lungs and tissues. *Pharmacol Rev.* 1951;3(1):1–41.
39. Morgan DJ, Huang JL. Effect of plasma protein binding on kinetics of capillary uptake and efflux. *Pharm Res.* 1993;10(2):300–4.
40. Schneck DW, Pritchard JF, Hayes A. Studies on the uptake and binding of propranolol by rat tissues. *J Pharmacol Exp Ther.* 1977;203(3):621–9.
41. Yang KH, Choi YH, Lee U, Lee JH, Lee MG. Effects of cytochrome P450 inducers and inhibitors on the pharmacokinetics of intravenous furosemide in rats: involvement of CYP2C11, 2E1, 3A1 and 3A2 in furosemide metabolism. *J Pharm Pharmacol.* 2009;61(1):47–54.
42. Berry LM, Li C, Zhao Z. Species differences in distribution and prediction of human V_{ss} from preclinical data. *Drug Metab Dispos.* 2011;39(11):2103–16.
43. Yang SH, Choi HG, Lim S-J, Lee MG, Kim SH. Effects of morin on the pharmacokinetics of etoposide in 7, 12-dimethylbenz [a] anthracene-induced mammary tumors in female Sprague-Dawley rats. *Oncol Rep.* 2013;29(3):1215–23.
44. Ueda K, Kato Y, Komatsu K, Sugiyama Y. Inhibition of biliary excretion of methotrexate by probenecid in rats: quantitative prediction of interaction from in vitro data. *J Pharmacol Exp Ther.* 2001;297(3):1036–43.
45. Nishimura T, Kato Y, Amano N, Ono M, Kubo Y, Kimura Y, et al. Species difference in intestinal absorption mechanism of etoposide and digoxin between cynomolgus monkey and rat. *Pharm Res.* 2008;25(11):2467–76.
46. Kerns EH, Di L, Petusky S, Farris M, Ley R, Jupp P. Combined application of parallel artificial membrane permeability assay

- and Caco-2 permeability assays in drug discovery. *J Pharm Sci.* 2004;93(6):1440–53.
47. Saitoh R, Sugano K, Takata N, Tachibana T, Higashida A, Nabuchi Y, et al. Correction of permeability with pore radius of tight junctions in Caco-2 monolayers improves the prediction of the dose fraction of hydrophilic drugs absorbed by humans. *Pharm Res.* 2004;21(5):749–55.
 48. Fremstad D, Jacobsen S, Lunde PK. Influence of serum protein binding on the pharmacokinetics of quinidine in normal and anuric rats. *Acta Pharmacol Toxicol.* 1977;41(2):161–76.
 49. D'Argenio DZ, Schumitzky A, Wang X. ADAPT 5 user's guide: pharmacokinetic/pharmacodynamic systems analysis software. Los Angeles: Biomedical Simulations Resource; 2009.
 50. Jusko WJ, Li X. Assessment of the Kochak-Benet equation for hepatic clearance for the parallel-tube model: relevance of classic clearance concepts in PK and PBPK. *AAPS J.* 2022;24:5
 51. Trapp S, Rosania GR, Horobin RW, Kornhuber J. Quantitative modeling of selective lysosomal targeting for drug design. *Eur Biophys J.* 2008;37(8):1317.
 52. Pang KS, Han YR, Noh K, Lee PI, Rowland M. Hepatic clearance concepts and misconceptions: why the well-stirred model is still used even though it is not physiologic reality? *Biochem Pharmacol.* 2019;169:113596.
 53. Chapa R, Li CY, Basit A, Thakur A, Ladumor MK, Sharma S, et al. Contribution of uptake and efflux transporters to Oral pharmacokinetics of furosemide. *ACS omega.* 2020;5(51):32939–50.
 54. Chennavasin P, Seiwel R, Brater DC, Liang WM. Pharmacodynamic analysis of the furosemide-probenecid interaction in man. *Kidney Int.* 1979;16(2):187–95.
 55. Smith DE, Gee WL, Brater DC, Lin ET, Benet LZ. Preliminary evaluation of furosemide–probenecid interaction in humans. *J Pharm Sci.* 1980;69(5):571–5.
 56. Shen H, Holenarsipur VK, Mariappan TT, Drexler DM, Cantone JL, Rajanna P, et al. Evidence for the validity of pyridoxic acid (PDA) as a plasma-based endogenous probe for OAT1 and OAT3 function in healthy subjects. *J Pharmacol Exp Ther.* 2019;368(1):136–45.
 57. Sakurai Y, Motohashi H, Ueo H, Masuda S, Saito H, Okuda M, et al. Expression levels of renal organic anion transporters (OATs) and their correlation with anionic drug excretion in patients with renal diseases. *Pharm Res.* 2004;21(1):61–7.
 58. Levitt DG. Physiologically based pharmacokinetic modeling of arterial–antecubital vein concentration difference. *BMC Clin Pharmacol.* 2004;4(1):1–23.
 59. Benet LZ. The role of BCS (biopharmaceutics classification system) and BDDCS (biopharmaceutics drug disposition classification system) in drug development. *J Pharm Sci.* 2013;102(1):34–42.
 60. Benet LZ, Broccatelli F, Oprea TI. BDDCS applied to over 900 drugs. *AAPS J.* 2011;13(4):519–47.
 61. Scheufler E. Evidence for nonlinear pharmacokinetics of methotrexate in the rat. *Pharmacology.* 1982;25(1):51–6.
 62. Li X, Choi J-S. Effects of quercetin on the pharmacokinetics of etoposide after oral or intravenous administration of etoposide in rats. *Anticancer Res.* 2009;29(4):1411–5.
 63. Piekoszewski W, Chow FS, Jusko WJ. Disposition of tacrolimus (FK 506) in rabbits. Role of red blood cell binding in hepatic clearance. *Drug Metab Dispos.* 1993;21(4):690–8.
 64. Tucker G, Casey C, Phillips P, Connor H, Ward J, Woods H. Metformin kinetics in healthy subjects and in patients with diabetes mellitus. *Br J Clin Pharmacol.* 1981;12(2):235–46.

Publisher's Note Springer Nature remains neutral with regard to jurisdictional claims in published maps and institutional affiliations.